Colloids and Surfaces A: Physicochemical and Engineering Aspects 727 (2025) 138120

Contents lists available at ScienceDirect

Colloids and Surfaces A: Physicochemical and Engineering Aspects

journal homepage: www.elsevier.com/locate/colsurfa

Biomimicking extracellular matrix fabricated from alginate-polypeptide hydrogel with aligned fibrous structure

Dun-Heng Tan [a], Chun-Yu Chang [b,c,*], Yu-Ching Huang [c,d,**], Meng-Fang Lin [c,d], Wei-Fang Su [a,d,***]

[a] Department of Materials Science and Engineering, National Taiwan University, Taiwan
[b] Bachelor Program in Semiconductor Materials and Fabrication, Ming Chi University of Technology, Taiwan
[c] Biochemical Technology R&D Center, Ming Chi University of Technology, Taiwan
[d] Department of Materials Engineering, Ming Chi University of Technology, Taiwan

GRAPHICAL ABSTRACT

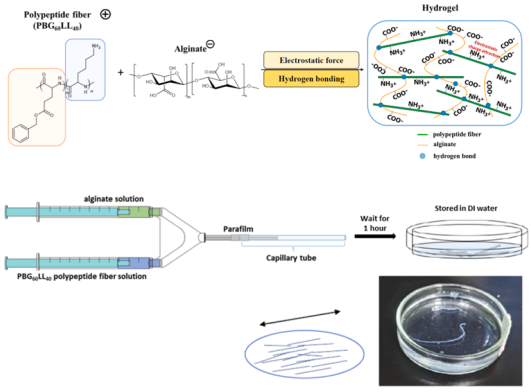

ARTICLE INFO

Keywords:
Alginate
Polypeptide
Aligned structure
Hydrogel
Co-extrusion
Mechanical properties
Biocompatibility

ABSTRACT

Hydrogels are promising scaffold materials for tissue engineering due to their adjustable mechanical properties and excellent biocompatibility. The soft nature and high water content of hydrogels demonstrate their potential to mimic the extracellular matrix (ECM), providing an environment similar to that in vivo for cell biology. However, conventional hydrogels are typically isotropic, which limits their ability to guide cell growth required for neural tissue engineering. In this study, we developed a novel alginate-polypeptide hydrogel with an aligned fibrous structure to address this limitation. Alginate is a naturally abundant biocompatible carbohydrate polymer, which was selected for its ability to form hydrogels Simultaneously, we synthesized copolypeptides with glutamate and lysine moieties, where glutamate stimulates nerve regeneration while lysine enhances cell adhesion and adjusts charges for effective crosslinking. The copolypeptides were electrospun to form fibers, which were subsequently selectively deprotected to acquire positive charged fibers, enabling electrostatic

* Corresponding author at: Bachelor Program in Semiconductor Materials and Fabrication, Ming Chi University of Technology, Taiwan.
** Corresponding author at: Biochemical Technology R&D Center, Ming Chi University of Technology, Taiwan.
*** Corresponding author at: Department of Materials Science and Engineering, National Taiwan University, Taiwan.
E-mail addresses: changcy@mail.mcut.edu.tw (C.-Y. Chang), huangyc@mail.mcut.edu.tw (Y.-C. Huang), suwf@ntu.edu.tw (W.-F. Su).

https://doi.org/10.1016/j.colsurfa.2025.138120
Received 8 July 2025; Received in revised form 3 August 2025; Accepted 21 August 2025
Available online 21 August 2025

crosslinking with negatively charged alginate. The resulting hydrogel exhibited an aligned fibrous structure achieved through the shearing force of co-extrusion method, as confirmed by polarized optical microscope (POM) and transmission X-ray microscopy (TXM). This resulting hydrogel possesses greater mechanical strength than the alginate-calcium hydrogel control group even when both has the same charge density. This enhancement arises from chain entanglement and hydrogen bonding between alginate and polypeptide. Finally, the cell viability tests and cytotoxicity tests confirm that the hydrogel has good biocompatibility for biomedical applications.

1. Introduction

Hydrogels are materials formed from polymer networks that create three dimensional hydrophilic structures capable of absorbing large amounts of water. Their unique properties have attracted significant attention in various fields [1–5]. In biomedical applications, hydrogels are particularly promising as scaffold materials due to their excellent mechanical properties and biocompatibility. Their ability to mimic the extracellular matrix (ECM) and support cell growth makes them ideal for advanced tissue engineering applications [6–12]. The ECM refers to a composite structure of macromolecules that supports cells and tissues. It primarily consists of water and extracellular polymeric substances (EPS), including polysaccharides, fibrous proteins and DNA [13,14]. The ECM not only provides supportive structures but also carries the nutrition, hormones, and other signal molecules. The fibrous proteins in the ECM form a gel-like matrix that serve as a support structure for cells adhesion [15]. This fibrous structure is vital for providing structural support and strength in various tissues. For instance, the corneal tissue's ECM primarily consists of fibrous collagens, particularly types I and V, which are tightly packed with well-defined inter-fibril spacing [16]. The corneal stroma with a thickness of approximately 300–400 μm and constituting 80–90 % of the corneal volume, plays an important role in determining corneal characteristics [17]. The collagen fibers in the corneal stroma are highly organized in lamellae, providing strength and resistance to deformation. The precise arrangement of collagen fibers is crucial for the cornea's optical clarity. Another example is artery tissue, where the ECM is primarily composed of collagen and elastin fibers. These fibers provide the arterial wall with both strength and elasticity [18,19]. The fibers are arranged in a criss cross pattern, providing structural integrity and preventing the artery from over expansion under pressure. They also help maintain vascular tone, regulate blood pressure, and ensure proper blood flow to tissues and organs. Additionally, the fibrous tissue in the arterial wall anchors the artery in place, offering structural support to prevent vessel collapse or distortion [20–23].

To replicate the structure of the ECM in tissue engineering, incorporating fibrous components into hydrogels has emerged as a promising approach [24,25]. Fibrous structure in hydrogel plays an important role by provide an organized framework that supports cell adhesion, migration, and alignment, which are critical for proper tissue development and regeneration. Electrospinning enables the fabrication of fibrous structures that closely mimic the ECM in terms of size and architecture. By integrating electrospun scaffolds with hydrogels, three dimensional hybrid constructs can be created, providing a platform for tissue regeneration. Moreover, these electrospun fibers can also be designed to be protease-degradable, enhancing their biofunctionality and broadening their applications in tissue engineering [26–28].

While incorporating fibrous components in hydrogels offers significant benefits, the isotropic fiber arrangement still limits their ability to guide directional cell growth effectively. Hydrogels with aligned fiber structures are particularly beneficial as they provide directional guidance for cell migration and promote organized tissue formation, which is essential for regenerating tissues like tendons, nerves, and muscles. However, achieving fiber alignment within hydrogels presents significant challenges due to their viscous nature, the random distribution of polymer chains, and their lack of structural rigidity. Several innovative fabrication techniques have been developed to address these issues. For example, Formica et al. fabricated a composite hydrogel using cryo-electrospinning to create an ultraporous scaffold that mimics the structure of cartilage tissue [29]. This composite hydrogel demonstrated a sustained release profile of pharmaceutical agents that could rescue chondrocytes from an inflammatory environment. Similarly, Deepthi et al. designed a layered composite hydrogel enriched with aligned electrospun poly-L-lactic acid (PLLA) nanofibers to replicate the glycosaminoglycans-rich ECM of tendon sheaths, demonstrating similar cytocompatibility to native tissue and promoting oriented cell growth along the nanofibers for tendon regeneration [30]. Despite these advances, the complicated preparation process for creating hydrogels with aligned fiber structures still hinder their widespread adoption and scalability in practical applications. Therefore, we need to develop a simple and efficient method to fabricate hydrogel with aligned fiber structure, ensuring broader accessibility and utility in tissue engineering applications. Recent studies in catalysis and analytical chemistry have demonstrated that nanoscale alignment and well controlled interfacial interactions are critical for improving molecular recognition and enhancing the sensitivity and selectivity of functional materials [31–34]. These researches reflect a broader recognition that molecular level structural organization is essential in the design of advanced materials.

Alginate is a naturally derived polysaccharide obtained from brown seaweed and is widely used in biomedical applications, particularly for hydrogel fabrication in tissue scaffolds. It is highly biocompatible, non-toxic and non-immunogenic, making it ideal for cell culture and drug delivery in tissue engineering. Alginate can easily form hydrogels by crosslinking with divalent cations such as Ca^{2+} to create a stable three dimensional structure. This crosslinking process can be conducted without the use of organic solvents or high temperatures, which helps to protect cells or bioactive agents. Additionally, the mechanical properties of alginate can be tailored by adjusting its concentration or crosslinking density, enabling customization for specific biomedical applications. Its high water absorption capability mimics ECM, promoting cell growth and proliferation. Furthermore, alginate can be combined with other biomaterials or growth factors to enhance its biocompatibility or cell adhesion on scaffold [35]. B. Sarker et al. fabricated covalent cross-linked alginate hydrogels that demonstrated good cell adhesion and spreading. These hydrogels were synthesized through Schiff base formation between gelatin and alginic acid and showed increased mitochondrial activity compared to blend hydrogels [36].

Polypeptides are increasingly recognized as versatile building blocks for hydrogel formation and multicomponent matrix design in tissue engineering [37–39], owing to their excellent biodegradability, biocompatibility, and structural similarity to the extracellular matrix (ECM). Polypeptides can be synthetically engineered to precisely design the desired monomer composition and tailor physical and chemical properties to meet the needs of different kinds of tissues. By incorporating specific functional amino acid monomers, such as lysine for enhancing cell attachment and glutamate for stimulating nerve cell growth, polypeptides can be optimized for specialized tissue engineering applications. This versatility enables polypeptides to facilitate the development of hydrogels that not only provide structural support but also actively promote tissue regeneration. Tseng et al. developed a kind of anisotropic structured hydrogel scaffold by co-extrusion of cellulose nanofiber (CNF) solution and poly(L-lysine)-r-poly(L-glutamic acid)

polypeptide solution. The lysine moieties in the polypeptide provide positive charges that crosslink with negatively charged CNF. Meanwhile, the glutamic acid moieties stimulate nerve cells. The resulting hydrogel thus can promote cellular activity through the multifunctionality of the polypeptide [40]. In this context, aligned CNF plays an important role in guiding neurite growth. However, if we can replace CNF with aligned polypeptide fibers containing glutamic acid monomers, it may further enhance neurite guidance due to the inherent ability of glutamic acid to stimulate nerve cells. This approach could be more effective for neuronal growth and repair [41].

In this study, we synthesized copolypeptides containing glutamate and lysine moieties, where glutamate stimulates nerve regeneration while lysine enhances cell adhesion and adjusts charges to enable efficient crosslinking. Utilizing the unique properties of these copolypeptides, we developed a novel fabrication technique to create hydrogels with aligned fiber structures by combining alginate and electrospun copolypeptide fibers via electrostatic crosslinking. The process involved first preparing positively charged polypeptide fibers, followed by co-extrusion with negatively charged alginate. Controlled shear forces applied during extrusion facilitated the alignment of the polypeptide fibers in the direction of extrusion, resulting in hydrogels with an anisotropic fibrous architecture. Compared to conventional alignment methods such as electrospun fiber embedding [30] or freeze electrospinning [29], the co-extrusion approach used in this study offers several practical advantages. It avoids the need for organic solvents or cryogenic processing, reduces fabrication steps, and enables simultaneous fiber alignment and hydrogel formation by simple one step co-extrusion using aqueous solutions. This simple and scalable strategy is more suitable for making functional materials with highly ordered structures that are useful in the wide applications of tissue engineering scaffolds, catalysts, batteries. Characterization techniques such as polarized optical microscopy (POM) and transmission X-ray microscopy (TXM) confirmed the fibrous and anisotropic nature of the hydrogel, demonstrating its potential for mimicking the ECM. The aligned structure of the hydrogels makes them highly suitable for tissue engineering applications, particularly in supporting cell attachment and promoting directional cell growth.

2. Experimental section

2.1. Materials

The synthesis of the polypeptide $PBG_{60}BocL_{40}$ through N-carboxyanhydrides ring-opening polymerization (NCA-ROP) is described in supporting information section S1 and in Figure S1 to Figure S3 according to previously published reports [40,42]. The chemical structure of monomers, polymers, and partially hydrolyzed polypeptide fibers were characterized by proton nuclear magnetic resonance spectroscopy (^{1}H NMR) (Brucker; Avance III-500MHz). The ^{1}H NMR spectra of γ-benzyl-L-glutamate N-carboxyanhydride (BGNCA) and N-ε-Boc-L-lysine N-carboxyanhydride (BocLNCA) are shown in Figure S4 and Figure S5, respectively, while the ^{1}H NMR spectrum of $PBG_{60}BocL_{40}$ is shown in Figure S6. All reagents were of analytical grade and used as without further purification. L-Glutamic acid γ-benzyl ester and N-ε-Boc-L-lysine were purchased from AK Scientific while sodium was obtained from Sigma-Aldrich. Sodium alginate was purchased from Acros Organics (Lot #. A0376863, the M/G ratio is 1.056 and the molecular weight is 183 kDa). Calcium chloride ($CaCl_2$) and dimethylformamide were provided by Fisher Chemical, and benzene was purchased from Showa Chemical. Trifluoroacetic acid was supplied by Fluorochem, and a 0.5 % stabilized aqueous solution of ruthenium tetroxide (RuO_4) was acquired from Polysciences, Inc. All other chemicals for synthesis and hydrogel preparation were purchased from Acros Organic. Reagents used for cell studies included RPMI 1640 media powder (HyClone, Lot #. MF29518516C), horse serum (HS) (Gibco, Lot #. 2534239), fetal bovine serum (FBS) (VWR Life Science Seradigm, Lot #. 171K18), penicillin/streptomycin/ amphotericin B (PSA) (HyClone, Lot #. J190044), sodium bicarbonate (Sigma-Aldrich) and 37 %, reagent grade hydrochloric acid (Scharlau), which were used to prepare cell culture medium. Phosphate buffered saline tablets (PBS) were provided by Sigma-Aldrich. The AlamarBlue™ cell viability reagent (Invitrogen, Lot #. 2214489) and Dulbecco's modified eagle medium (DMEM) (Gibco, Lot #. 2519909) were used to prepare working solution for cell viability test. The LIVE/DEAD™ Viability/Cytotoxicity Kit (Invitrogen, Lot #. 2161809) was employed for the cytotoxicity test, containing a 4 mM Calcein-AM (CaAM) solution in dimethyl sulfoxide (DMSO) and a 2 mM Ethidium Homodimer-I (EthD-I) solution in a DMSO/H_2O mixture (1:4, v/v).

2.2. Nomenclature

The abbreviations for the two types of polypeptides are poly((γ-benzyl-L-glutamate)$_{6\ m}$-random-(N-ε-Boc-L-lysine)$_{4\ m}$) as $PBG_{60}BocL_{40}$ and poly((γ-benzyl-L-glutamate)$_{6\ m}$-random-(L-lysine)$_{4\ m}$) as $PBG_{60}LL_{40}$. The nomenclature of the hydrogels is based on the composition of the alginate and the crosslinker $CaCl_2$ or polypeptide fiber $PBG_{60}LL_{40}$, which are abbreviated as AG, Ca, and 64, respectively. The effective concentrations of the crosslinker and alginate solution are indicated after the corresponding ingredient. The prefixes ani- represents anisotropic hydrogel prepared by the co-extrusion method. For instance, ani-64–1-AG-1 refers to an anisotropic hydrogel made with 1 wt% $PBG_{60}LL_{40}$ and 1 wt% alginate aqueous solution.

2.3. Polypeptide fiber preparation

2.3.1. Electrospinning

The polypeptide fiber was prepared by the electrospinning method as described in our previous study [41]. A 20.0 wt% of $PBG_{60}BocL_{40}$ polypeptide solution was prepared with a co-solvent mixture of tetrahydrofuran (THF)/ dimethyl acetamide (DMAc) (v/v = 6/4). The electrospinning was conducted at a voltage of 20.0 kV with a needle-to-collector distance of 10.0 cm and the collector rotating at 1500 rpm. After electrospinning, the nonwoven fibrous mat $PBG_{60}BocL_{40}$ was carefully removed from the parchment paper and stored at −20℃.

2.3.2. Selective deprotection

The electrospun polypeptide fibers were subjected to selective deprotection to remove the Boc-protecting groups. The deprotection was carried out by reacting the fibers with trifluoroacetic acid (TFA) in deionized water (DI water) overnight. The removal of the Boc-protecting groups was confirmed by ^{1}H NMR analysis (Figure S7). Following deprotection, the fiber was purified by dialysis (MW cutoff = 3000 Dalton) in DI water until the pH value became neutral. The purified polypeptide fiber was then freeze-dried for 3 days and stored at −20℃ for further use in hydrogel preparation.

2.4. Hydrogel preparation

The deprotected polypeptide fiber $PBG_{60}LL_{40}$ was dispersed in DI water using magnetic stirring for at least 2 days to prepare 1.0 wt% and 2.0 wt% solutions. The hydrogel fabrication method was modified according to our previous study [40]. Hydrogels were fabricated in 12-well plates and 48-well plates for various studies. Take hydrogel fabricated in 48-well plate for example, 150 μL of $PBG_{60}LL_{40}$ solution was first injected into the well, followed by gently dropping the alginate solution onto the surface of the polypeptide fiber solution. The hydrogel was then placed at room temperature for at least 24 h to ensure complete gelation. The hydrogel was washed twice with DI water to remove excess alginate solution and immersed in DI water to prevent drying. $CaCl_2$ was served as control group to replace polypeptide fiber $PBG_{60}LL_{40}$. To meet the same charge density for the $PBG_{60}LL_{40}$ aqueous solution, calcium

chloride solution were prepared at concentrations of 10.94 mM and 21.88 mM, corresponding to the 1.0 wt% and 2.0 wt% $PBG_{60}LL_{40}$ aqueous solutions, respectively.

To observe the semi-crystalline fibers formed in the hydrogels, anisotropic hydrogels were prepared using a co-extrusion method (Fig. 4). These hydrogels were fabricated by applying shear force through a syringe to align the polypeptide solution. A co-extrusion system equipped with 5.7 cm parallel needles and a capillary tube connected to the end of needles was employed for this process. $PBG_{60}LL_{40}$ aqueous solutions (1.0 wt% or 2.0 wt%) and alginate aqueous solutions (1.0 wt% or 2.0 wt%) were used to fabricate the hydrogel. Each solution (100 μL) was loaded into a 1 mL syringe, and the syringes were connected to the co-extrusion setup. A steady, controlled shear force was applied through the needle and capillary tube extension during extrusion. Gelation began when the two solutions met in the capillary tube. To prevent polymer relaxation of the polymer chains during gelation, the hydrogel was kept in the capillary tube for at least one hour. The resulting anisotropic hydrogels were then stored in petri dishes containing DI water.

2.5. Hydrogel characterization

2.5.1. Scanning electron microscope (SEM)

Hitachi S-3400N SEM was utilized to obtain SEM images. Hydrogel samples were freeze-dried prior to imaging. The dried hydrogel samples were cut with a scalpel blade to obtain the cross-sections, and then the samples were stuck on the holder with carbon tape. The holder with the dried hydrogel samples was coated with platinum by sputtering for 20 s.

2.5.2. Polarized optical microscope (POM)

POM images were obtained using Leica Microsystems DM 2500 M. Anisotropic hydrogel samples prepared via the co-extrusion method were carefully sliced into thin sections with a thickness of approximately 10–20 μm using a microtome to allow sufficient light transmission during observation. The sections were then mounted on glass slides and covered with cover slips to prevent dehydration. Samples were placed between two polarizers to acquire POM images and observed under both parallel mode and cross-polar mode. A 550 nm quartz compensator was used under cross-polar mode to enhance birefringence contrast.

2.5.3. Transmission X-ray microscope (TXM)

The three dimensional tomography TXM images of hydrogels were taken at TLS01B1 work station at the National Synchrotron Radiation Research Center (NSRRC), Taiwan. The hydrogel sample was stained with RuO_4 solution to enhance contrast under TXM by oxidizing carbon and nitrogen atoms. After 24 h of staining, the RuO_4 solution was removed, and the hydrogel was rinsed with DI water three times. The hydrogel was then soaked in DI water to prevent drying. The stained hydrogel sample was peeled and stuck on the special iron sheet with Kapton tape (3 M Co.). A solution of gold nanoparticles (with diameters ranging from 400 to 500 nanometers) was applied to the stained hydrogel sample as anchor points for the tomography images, and then the sample was sealed with another piece of Kapton tape. Thin samples were necessary for the proper focusing of TXM in order to achieve high resolution images.

2.5.4. Water content

Hydrogels were fabricated inside the 5 mL vial bottles, which were weighed before use. After complete gelation, the hydrogels were rinsed with DI water twice to remove the excess solution. Both wet and freeze-dried hydrogels were weighed along with their vial bottles. The water content of the hydrogel was calculated using the following formula:

$$\text{water content } (\%) = \frac{W_{wet} - W_{dry}}{W_{wet}}$$

where W_{wet} and W_{dry} are the weights of the vial containing the wet and freeze-dried hydrogels, respectively.

2.5.5. Characterization of mechanical properties

The mechanical properties of hydrogels were determined using TA instruments rheometer AR2000Dex. Hydrogel samples were placed on the rheometer plate, and a 20 mm parallel plate geometry was lowered to 800 μm. The samples were squeezed by the parallel plate, and the excess hydrogel was removed. The test was conducted at 25℃ with a strain set to 0.1 %. The angular frequency sweeping was performed from 0.1 rad/s to 10.0 rad/s.

2.5.6. Dynamic light scattering

The zeta potential and particle size of $PBG_{60}LL_{40}$ fiber suspensions were measured using a Brookhaven BI-90 Plus Particle Size Analyzer (Brookhaven Instruments, USA). The fibers were dispersed in deionized water to prepare a 0.01 wt% homogeneous solution. Measurements were performed using dynamic light scattering technique at room temperature. Each sample was measured five times, and the mean values along with standard deviations were reported.

2.6. In vitro cell culture

2.6.1. Cell culture

Pheochromocytoma 12 (PC12) cell lines were utilized for the cell experiments. The cells were provided by Prof. Jia-Shing Yu, Department of Chemical Engineering, National Taiwan University. Different wells of tissue culture polystyrene (TCPS) cell culture plates (Corning Falcon, product #. 353078) were used for cell culture experiments. The RPMI-1640 medium was prepared by dissolving 5.2 g of RPMI-1640 powder in 420.0 mL double-distilled water, followed by the addition of 1.0 g of sodium bicarbonate. The pH value was adjusted to 7.4 using 1 M $HCl_{(aq)}$, Afterward, 50.0 mL of HS, 25.0 Ml of FBS, and 5.0 mL PSA were added sequentially. The cells were cultured in this RPMI-1640 medium at 37℃ under 5 % CO_2. In addition, a PBS solution was prepared by dissolving a PBS tablet in 200.0 mL of double-distilled water and sterilized by autoclaving at 121℃ for 30 min. T75 flasks were used for cell culture, and the culture medium was replaced every 72 h after washing the flasks with 5.0 mL of 37°C PBS solution. Fresh 10.0 mL of RPMI-1640 medium was then added to maintain optimal cell growth and ensure consistent experimental conditions.

2.6.2. Cell viability

The Alamar Blue assay was conducted to assess the cell viability test of hydrogels on Day 2, Day 4, and Day 6. The AlamarBlue™ cell viability reagent (Invitrogen, Lot #. 2214489) was diluted with DMEM to prepare a 10 % (v/v) working solution. After replacing the medium with the working solution, the samples were incubated at 37°C for 3 h. Following incubation, the working solution was transferred to a 96-well plate and separated into 100 μL per well. Each sample was collected in triplicate (3 ×100 μL) for the fluorescent test (n = 9 for each hydrogel). Absorbance at 570 nm and 600 nm were measured respectively by a microplate reader (BioTek 800 TS). The calculation details are provided in the supporting information **section S2**.

2.6.3. Cytotoxicity

The Live/Dead assay was used to determine the cytotoxicity of hydrogels. The assay was performed after culturing PC12 cells on hydrogels, with coverslips serving as the control. The LIVE/DEAD™ Viability/Cytotoxicity Kit (Invitrogen, Lot #. 2161809) was used in this study. The working solution for the Live/Dead assay was prepared by mixing 6 μL of Calcein-AM (CaAM) solution, 24 μL of Ethidium Homodimer-I (EthD-I) solution, and 12.0 mL of 37℃ PBS in a centrifuge tube, which was then wrapped with aluminum foil to protect it from light. 400 μL of the staining solution was added to each well, and the well plate was also wrapped with aluminum foil to protect it from light.

The well plate was gently shaken by a digital shaker for 30 min, and then the staining solution was carefully removed. Samples were washed with 37℃ PBS twice, and 50 μL of PBS was added to prevent hydrogel from desiccation. Samples were observed using a fluorescent microscope (Leica Microsystems DMI3000 B). Due to the rough surface of hydrogels, it was challenging to capture high-quality fluorescent images of live and dead cells. Therefore, the ratio of live to dead cells was determined by counting the number of each type. Three sections were captured for each hydrogel and cells from a total of nine images were counted per sample. For each sample, at least 300 cells were counted to determine the Live/Dead results.

3. Results and discussion

Hydrogels are ideal for tissue engineering applications due to their softness, high water content, and excellent biocompatibility. Electrospinning is a widely used method for creating fibrous structures that mimic the native ECM, providing scaffolds suitable for biomedical use. Hydrogels with fibrous structure can not only modulate mechanical properties but also promote cell attachment, making them promising materials for tissue engineering. Recent advances in supramolecular hydrogel design further emphasize the importance of hydrogen bonding and electrostatic interactions in constructing functional and biologically relevant fibrous matrices for tissue engineering applications [43]. In this study, we aimed to develop a novel hydrogel with an aligned fibrous structure by utilizing partially hydrolyzed of polypeptide fibers $PBG_{60}BocL_{40}$ and crosslinking them with alginate via electrostatic charges. The polypeptide copolymer $PBG_{60}BocL_{40}$ is synthesized in our lab using ring opening copolymerization of anhydride monomers of PBG and Boc-polylysine [44]. After selectively deprotecting the Boc-protecting groups of polylysine, the polypeptide fibers $PBG_{60}LL_{40}$ acquired a positive charge, enabling electrostatic crosslinking with negatively charged alginate to form hydrogels with fibrous structure. The fabrication scheme is shown in Fig. 1.

The ion-free fiber $PBG_{60}BocL_{40}$ was prepared by electrospinning, and the SEM images of the $PBG_{60}BocL_{40}$ fiber are shown in Fig. 2**(a)** and **(b)**. The diameters range from approximately 400 to 600 nm. Then the polyelectrolyte fiber $PBG_{60}LL_{40}$ was obtained by selectively deprotecting $PBG_{60}BocL_{40}$ fiber with TFA to remove the Boc-protecting group. The completion of this deprotection process was confirmed by ^{1}H NMR, as shown in Figure S7**.** Fig. 3 illustrates the chemical structure of the polypeptide before and after deprotection, along with a photo of the final freeze-dried $PBG_{60}LL_{40}$, demonstrating that the deprotected $PBG_{60}LL_{40}$ still retains its fibrous structure. Following deprotection, the $PBG_{60}LL_{40}$ fibers were redispersed in DI water. The amine groups of the lysine repeat units impart positive charges to the fiber, as indicated by dynamic light scattering. The polyelectrolyte fiber $PBG_{60}LL_{40}$ has a zeta potential of 47.09 ± 2.10 mV and particle size of 339.0 ± 10.8 nm, making it a stable suspension in water, which is also shown in Fig. 3. The positive charge of the polypeptide fiber allows it to be crosslinked with negatively charged alginate via electrostatic force, forming the hydrophilic polymeric network.

The fabrication of the hydrogel was optimized to create a flat surface and steady gelation during the crosslinking process. The slow and steady gelation was controlled by gently dropping the alginate solution onto the $PBG_{60}LL_{40}$ polypeptide fiber solution. The hydrogel was fabricated on a coverslip for demonstration, as shown in Fig. 4**(a)**. In addition, to observe the semi-crystalline fibers formed in the hydrogels, we also prepare the anisotropic hydrogels. Fig. 4**(b)** illustrates the preparation of hydrogel with an aligned structure using the co-extrusion [40] of alginate solution and $PBG_{60}LL_{40}$ polypeptide fiber solution**.**

To confirm the fibrous structure within the hydrogel, the cross-sectional SEM images were taken. After freeze drying the 64–2-AG-2 hydrogel sample and sputtering it with platinum, the fibrous structure was observed under SEM, as shown in Fig. 5**(a)** and **(b)**. The fibrous structure originated from the $PBG_{60}LL_{40}$ fibers, while the sheet-like structure resulted from the crosslinked alginate. The presence of the aligned fibrous structure mimics the morphology of the native extracellular matrix, which supports cell adhesion and influences cellular behavior, suggesting that this hydrogel has strong potential to promote cell attachment in tissue engineering applications [45]. The formation of the fibrous hydrogel is primarily governed by a combination of electrostatic interactions and hydrogen bonding between the alginate and polypeptide chains. The positively charged ε-amino groups of lysine residues along the polypeptide backbone interact ionically with the negatively charged carboxyl groups of alginate, resulting in stable electrostatic crosslinking. In addition, hydrogen bonds are expected to form between the amide groups of the polypeptide and both hydroxyl and carboxyl functional groups on the alginate chains. These non-covalent interactions collectively contribute to the structural integrity and stability of the hydrogel network. The combination of electrostatic interactions and hydrogen bonding is particularly important for maintaining the alignment and mechanical robustness of the fibrous structure during gelation and subsequent processing.

To characterize the true structure of wet hydrogels, POM was utilized to observe the optical properties of fibrous hydrogels, as shown in Fig. 6 **(a)** to **(d)**. POM allowed for detailed observation of the fibrous structure within the hydrogels, revealing that the semi-crystalline structure of the orderly aligned fibers imparts specific optical properties. The cross-polar setup of the POM enables the observation of birefringence in samples. With an additional compensator placed between the sample and the analyzer, non-birefringent domains appear pink or purple, while birefringent regions display colors such as red or blue, depending on the orientation of the crystalline structure. The fibrous structure originates from the electrospun fibers dispersed in water; hence, the modifications in the hydrogel fabrication process can arrange these fibers into specific patterns. In this study, co-extrusion anisotropic hydrogels demonstrated the ability to rearrange the fiber alignment into a defined structure. The stress applied during extrusion caused the fibers to align in the direction of extrusion, resulting in the anisotropic samples exhibit strong

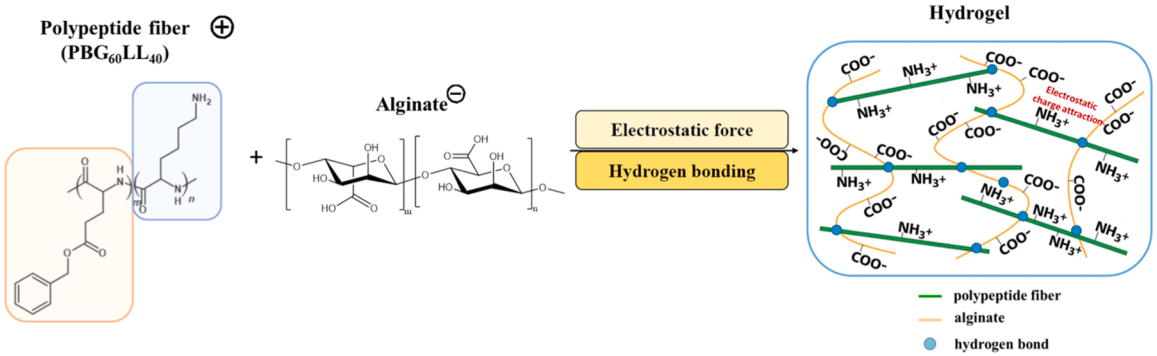

Fig. 1. Scheme for the preparation and chemical structure of hydrogel with fibrous structure.

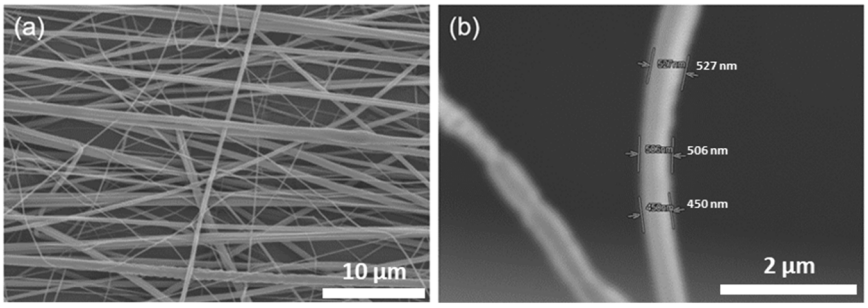

Fig. 2. SEM images of electrospun fiber $PBG_{60}BocL_{40}$ under (a) 3,000x, and (b) 20,000x magnification.

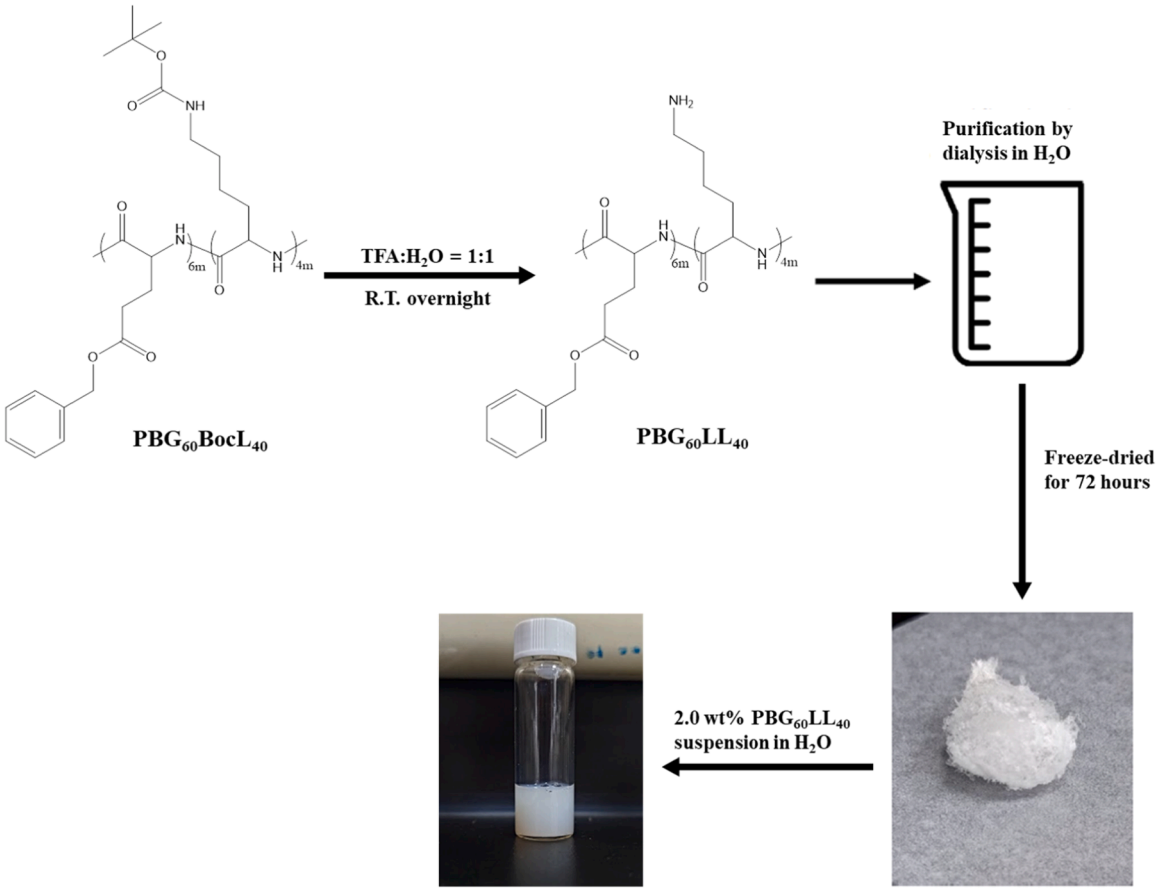

Fig. 3. Deprotection of $PBG_{60}BocL_{40}$ fiber to $PBG_{60}LL_{40}$ fiber and the subsequent preparation of $PBG_{60}LL_{40}$ suspension in DI water.

birefringent behavior compared to isotropic sample under POM. A uniform structure was observed in the co-extrusion anisotropic hydrogels (Fig. 6 **(c)** and **(d)**) whereas the isotropic hydrogel displayed only a local crystalline structure within the hydrogel samples (Fig. 6 **(a)** and **(b)**).

Although POM reveals the presence of crystalline structures at the micro-scale, it was insufficient to demonstrate the ordered fibrous architecture at nano or sub-micron range of the hydrogel. To achieve more precise observation of the fibrous structure, TXM was employed for the sub-micron scale analysis. TXM can visualize the structure of wet hydrogels from multiple angles with a resolution down to hundreds of nanometers. RuO_4 staining was applied to enhance the contrast between organic materials and water. The images collected from different angles were then used to simulate a three dimensional model of the hydrogel. The fibrous structure of the 64–1-AG-1 hydrogel was observed from various TXM image angles, as shown in Fig. 7**(a)** and **(b)**. The sub-micron fibers in the hydrogel exhibited diameters ranging from 400 to 600 nm, closely matching those of the original electrospun fibers. This well-organized fibrous architecture demonstrated its potential to serve as a biomedical scaffold for tissue engineering applications, particularly where aligned structures of ECM are required, such as in neural and muscle tissue engineering.

For hydrogel used as scaffolds in tissue engineering, water content is an important parameter that reflects hydrophilicity, which directly influences the cell culture environment. In general, scaffolds with higher hydrophilicity exhibit greater biocompatibility for tissue engineering applications [46–48]. Three replicates were prepared for each group, and the standard deviation was calculated. The water content results are shown in Fig. 8**(a)** and **(b)**. For the composite hydrogel made from alginate and polypeptide $PBG_{60}LL_{40}$, the water content decreased as the concentration of the precursor solution increased. In contrast, for the composite hydrogel composed of alginate and calcium ions, Ca-2-AG-1

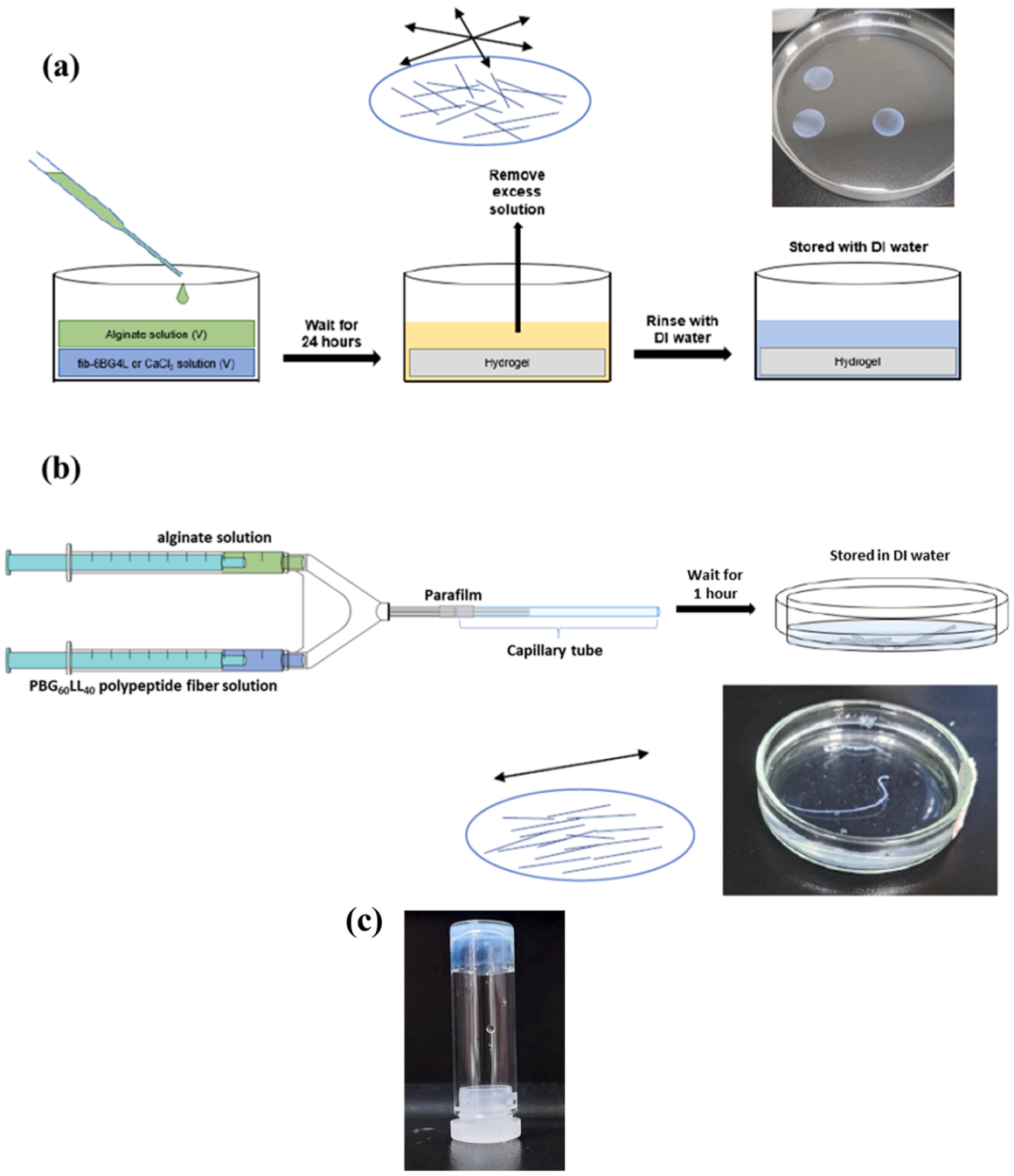

Fig. 4. Preparation of hydrogel (a) on 12-mm coverslip in a 10-cm Petri dish, and (b) with an aligned fiber structure using co-extrusion method. (c) Inverted tube test for the hydrogels.

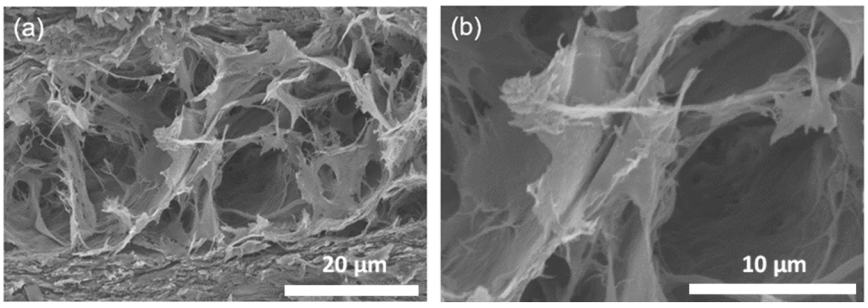

Fig. 5. SEM images of composite hydrogel 64–2-AG-2 under (a) 2,000x, and (b) 5,000x magnification.

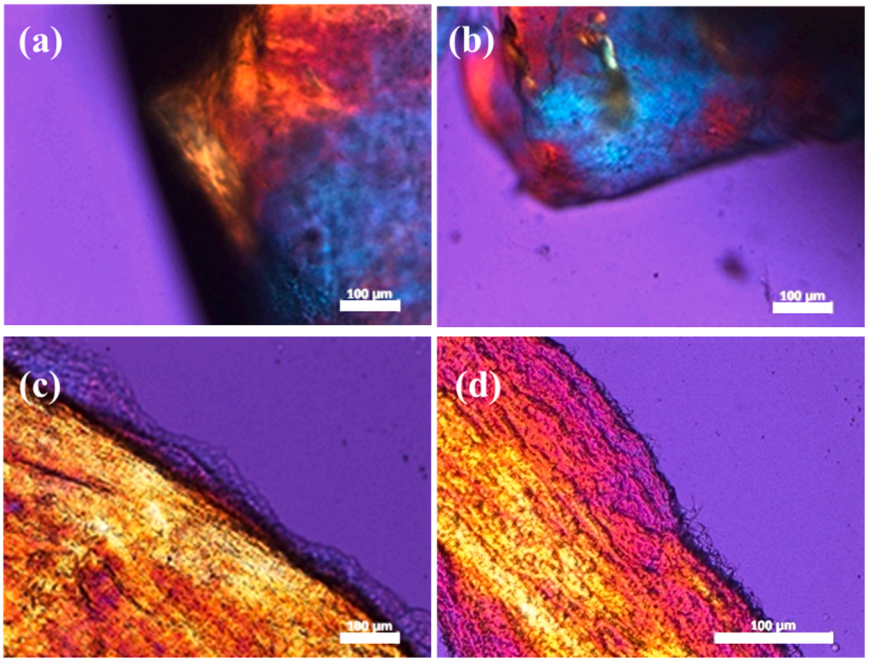

Fig. 6. POM images of wet hydrogel isotropic samples of (a) 64–1AG-1, (b) 64–2-AG-2, and anisotropic samples of (c) ani-64–1-AG-1 and (d) ani-64–2-AG-2 under cross-polar with compensator setup.

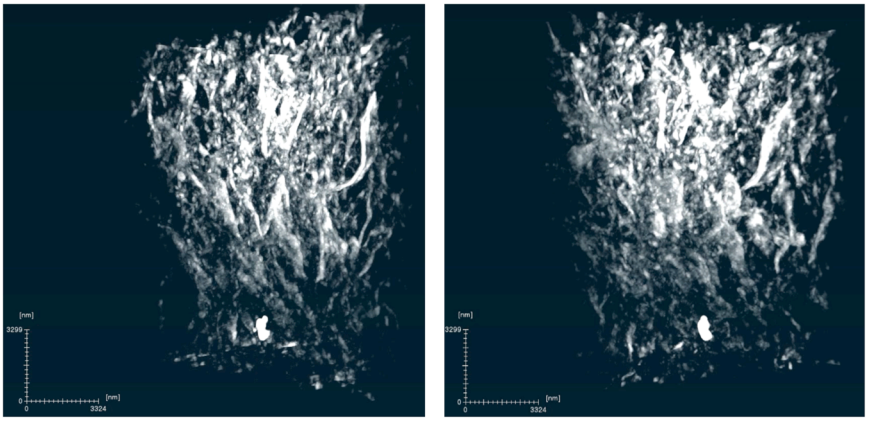

Fig. 7. TXM images of the wet hydrogel 64–1-AG-1 containing aligned fibers at (a) 45 ° and (b) 100°.

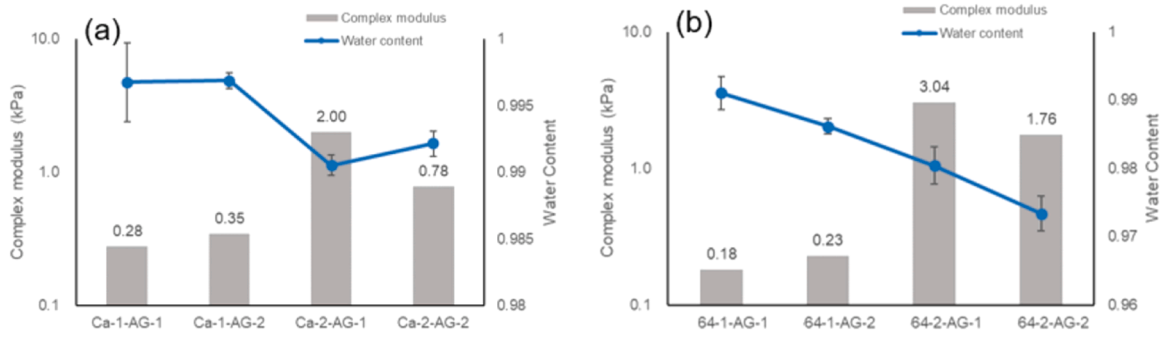

Fig. 8. Relation between water content and mechanical properties (complex modulus) of (a) alginate-calcium and (b) alginate-polypeptide hydrogels.

had the lowest water content. This is likely because an excess of calcium ions caused full crosslinking of the alginate, leading to a denser hydrogel network. In the case of Ca-2-AG-2 and other hydrogels, the alginate was present in excess, and the available calcium ions were insufficient to fully crosslink the alginate, resulting in higher water content.

Hydrogels are hydrophilic polymers that form a three dimensional network and can absorb significant amounts of water. Due to their semi-fluid nature, their mechanical properties are often characterized by

rheological measurements. In dynamic mechanical analysis, the material's mechanical behavior under shear stress is commonly described by the complex modulus, denoted as G. This modulus consists of the storage modulus (G′) and the loss modulus (G″), expressed by the equation $G = G' + iG''$. The storage modulus represents the elastic component of the viscoelastic hydrogel, indicating its ability to store energy, while the loss modulus reflects the viscous properties, representing energy dissipation. The ratio between storage and loss modulus is defined as the loss tangent (tanδ), which provides a measurement of the damping in the viscoelastic material as $\tan\delta = G''/G'$. A tan δ value close to zero indicates a predominantly elastic or solid-like behavior, whereas a value approaching 1 suggests a more viscous or liquid-like response.

The mechanical properties of alginate-calcium and alginate-polypeptide hydrogels are illustrated in Fig. 8(a) and (b) and summarized in Table 1. The strain sweep results of both types of hydrogels are presented in Figure S8. The measurements were taken at an angular frequency of 1.0 rad/s with 0.1 % strain, which falls within the linear viscoelastic region (LVR) for all samples. The complex modulus of alginate–calcium hydrogels ranged from 276.77 Pa (Ca-1-AG-1) to 2003.68 Pa (Ca-2-AG-1), reflecting a significant increase in stiffness with higher calcium ion concentrations. Among these, Ca-2-AG-1 exhibited the highest complex modulus and a relatively high tan δ value of 0.17, suggesting a more pronounced viscous contribution despite its high crosslinking density. In contrast, alginate–polypeptide hydrogels displayed a broader range of mechanical properties, with complex moduli spanning from 181.43 Pa (64–1-AG-1) to 3037.05 Pa (64–2-AG-1). The sample 64–2-AG-1, which had the same charge concentration as Ca-2-AG-1, demonstrated the highest mechanical strength among the polypeptide-containing hydrogels. This enhancement is likely due to increased chain entanglement and intermolecular interactions between alginate and polypeptide chains at higher concentrations. Notably, the tan δ values for alginate–polypeptide hydrogels ranged from 0.09 to 0.17, indicating comparable viscoelastic behavior to the calcium-crosslinked systems. At lower concentrations, alginate–polypeptide hydrogels exhibited weaker mechanical performance than their calcium-crosslinked counterparts. However, at higher concentrations, particularly in 64–2-AG-1, the mechanical strength of alginate–polypeptide hydrogels slightly surpassed that of alginate–calcium hydrogels. This shift suggests that while ionic crosslinking governs the initial mechanical integrity, polymer–polymer interactions and entanglements play a dominant role in reinforcing the network at higher component loadings. Across both systems, the tan δ values remained below 0.2, indicating predominantly elastic behavior, although higher tan δ in some samples points to increased energy dissipation under deformation.

Regarding the relationship between water content and the complex modulus, alginate-calcium hydrogels showed an increased complex modulus as water content decreased, as illustrated in Fig. 8**(a)**. This indicates that higher crosslinking density in alginate-calcium hydrogels reduces water content and enhances mechanical properties. For the alginate-polypeptide hydrogel samples, 64–1-AG-1 and 64–1-AG-2 demonstrated that lower crosslinking densities resulted in higher water content and lower mechanical properties. Interestingly, 64–2-AG-1, despite having higher water content than 64–2-AG-2, it still exhibited superior mechanical properties. This is likely due to its high hydrogel density, which results from chain entanglement and hydrogen bonding between alginate and polypeptide. Therefore, even with higher water content, 64–2-AG-1 demonstrated better mechanical properties than 64–2-AG-2.

Table 1
Storage modulus, loss modulus, complex modulus and tanδ of hydrogels.

Sample	Storage modulus G′ (Pa)	Loss modulus G″ (Pa)	Complex modulus G (Pa)	tanδ
Ca−1-AG−1	275.59	25.51	276.77	0.09
Ca−1-AG−2	345.17	22.84	345.92	0.07
Ca−2-AG−1	1975.95	332.08	2003.68	0.17
Ca−2-AG−2	777.72	48.08	779.20	0.06
64–1-AG−1	179.69	25.04	181.43	0.14
64–1-AG−2	225.17	37.46	228.26	0.17
64–2-AG−1	3008.40	416.20	3037.05	0.14
64–2-AG−2	1753.99	160.01	1761.27	0.09

In vitro cell viability studies are essential for assessing the biocompatibility of tissue engineering scaffolds before conducting in vivo experiments. Notably, PC12 cells have been widely used as a neuronal cell model to study nerve regeneration. Thus, the evaluation of hydrogel performance using PC12 cells directly reflects the scaffold's potential in neural tissue engineering. The aligned fibrous hydrogel structure mimics the architecture of neural ECM and provides directional guidance for neurite extension. In this study, cell viability was evaluated using the Alamar Blue assay. In this assay, the blue-colored resazurin in the Alamar Blue solution is reduced into red-colored resorufin by the mitochondria of healthy live cells. A higher percentage of resazurin reduction indicates the greater biocompatibility of the hydrogel scaffolds. Hydrogels were fabricated in a 48-well polystyrene (PS) plate for the cell viability test, with a 48-well TCPS plate without coating serving as the positive control. Each hydrogel sample was tested in triplicate for calculation the standard error. On Days 2, 4, and 6 after seeding of PC12 cells, the reduced solutions from each sample were collected and analyzed its absorbance at 570 nm and 600 nm. The results of the cell viability test are shown in Fig. 9. To evaluate the cell viability of hydrogels, the percentage reduction in the control group TCPS plate on Day 2 was used as a reference point. Hydrogels with a percentage reduction greater than this reference point are considered to have good biocompatibility.

Alginate-calcium hydrogels exhibited poor biocompatibility due to the small size of crosslinker calcium ion. During cell culture, the surface of these hydrogels has been gradually washed off when replacing the medium, leading to poor cell attachment and generally low cell viability. In contrast, alginate-polypeptide hydrogels maintained their structure better during cell culture because they have higher chain entanglement and hydrogen bonding between alginate and polypeptides. Polypeptide hydrogels demonstrated significantly better cell viability compared to alginate-calcium hydrogels and TCPS plates. The lysine units on the surface of the polypeptide crosslinker can support cell adhesion, and the soft hydrogel surface may also enhance cell proliferation. Among the alginate-polypeptide hydrogels, 64–1-AG-1 showed relatively low cell viability, which may be due to its lower mechanical properties compared to other samples. While other alginate-polypeptide hydrogels did not show significant differences in cell viability, 64–2-AG-1 had slightly lower cell viability. The strong mechanical property of 64–2-AG-1 probably reduces the cell adhesion. Despite 64–2-AG-1 had lower cell viability on Day 4, it supported cell proliferation and showed increased cell viability by Day 6.

Cytotoxicity is also an important indicator to determine whether the hydrogel scaffold is suitable for biomedical applications. It is assessed by counting the ratio of live cells to dead cells. A hydrogel scaffold is considered to have low cytotoxicity if this ratio exceeds 50 %. The cytotoxicity test was performed using the Live/Dead assay on Day 6 after cell seeding on hydrogels and TCPS. The LIVE/DEAD™ Viability/Cytotoxicity Kit was utilized for this analysis, and the results are shown in Fig. 10. The cytotoxicity of the control TCPS plate was close to 50 %, indicating that TCPS plates can support cell growth but with some level of cytotoxicity. The cytotoxicity of alginate-calcium hydrogels was slightly lower than that of TCPS control, while the alginate-polypeptide

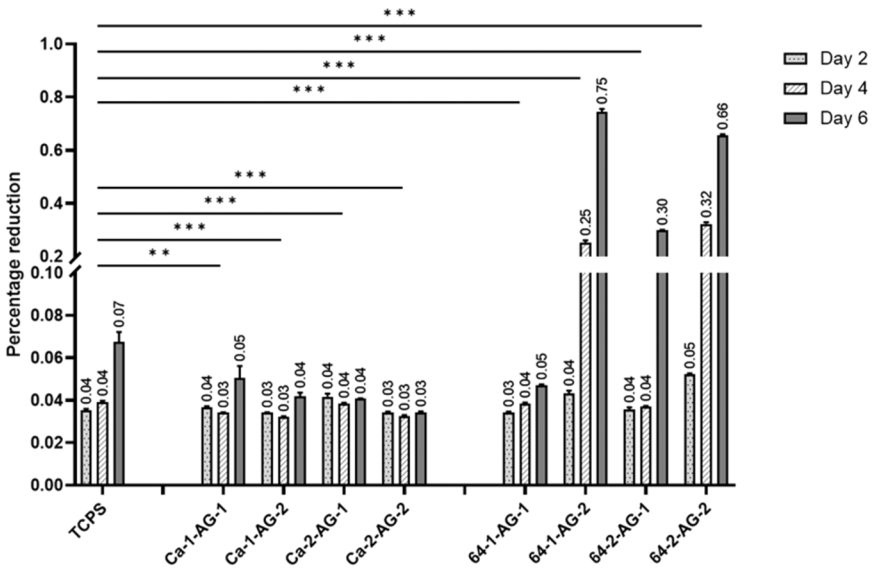

Fig. 9. Alamar blue assay of TCPS and hydrogels. The Kruskal-Wallis H-test was used to determine significant differences between groups. (* = $p < 0.05$, ** = $p < 0.01$, *** = $p < 0.001$).

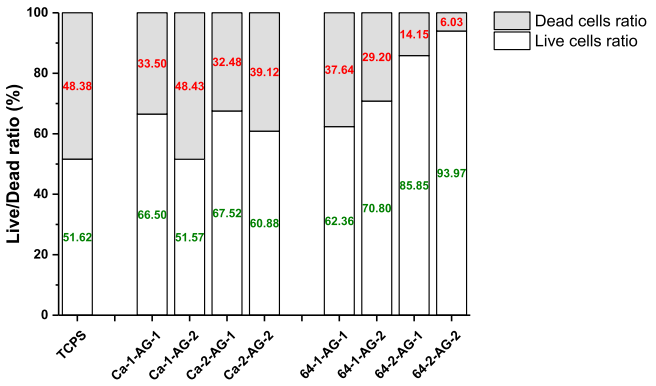

Fig. 10. Cytotoxicity test results of TCPS, alginate-calcium and alginate-polypeptide hydrogels.

hydrogels exhibited significantly lower cytotoxicity compared to TCPS. The results of the cytotoxicity test can relate to the cell viability test. Although alginate-calcium hydrogels had low cytotoxicity, they did not support cell growth effectively. In contrast, most alginate-polypeptide hydrogels except 64–1-AG-1 showed extremely low cytotoxicity and outstanding cell viability results. Overall, we conclude that the alginate-polypeptide hydrogels, particularly 64–2-AG-2, are suitable for biomedical applications as long as the crosslinking density and the concentration of the precursor solution are sufficiently high enough.

4. Conclusion

We successfully developed an innovative hydrogel with aligned fibrous structure by combining alginate and electrospun polypeptide fibers through electrostatic crosslinking. The aligned fibrous structure was achieved by applying controlled shear forces during the co-extrusion of positively charged polypeptide fibers and negatively charged alginate. This alignment of fiber structure within the hydrogel mimics the ECM architecture, which is critical for better supporting cell growth and guiding cell orientation in tissue regeneration applications. Characterization via SEM, POM, and TXM confirmed the highly organized fibrous structure within the hydrogels. Alginate-polypeptide hydrogels exhibit superior mechanical properties through chain entanglement and hydrogen bonding even with high water content. The alginate-polypeptide hydrogels also show remarkable biocompatibility, as evidenced by their significantly low cytotoxicity and high cell viability. The combination of the aligned fibrous structure, excellent mechanical properties, and outstanding biocompatibility suggests the potential of these hydrogels as promising scaffold materials for tissue engineering.

CRediT authorship contribution statement

Wei-Fang Su: Writing – review & editing, Supervision, Conceptualization. **Meng-Fang Lin:** Resources. **Yu-Ching Huang:** Resources, Project administration, Funding acquisition. **Chun-Yu Chang:** Writing – review & editing, Writing – original draft, Methodology. **Dun-Heng Tan:** Writing – original draft, Validation, Investigation.

Declaration of Competing Interest

The authors declare that they have no known competing financial interests or personal relationships that could have appeared to influence the work reported in this paper.

Acknowledgements

The authors highly appreciated the financial support obtained from National Science and Technology Council of Taiwan in this research (NSTC 113–2222-E-131–001, NSTC 114-2221-E-131-020-MY3, NSTC 112–2628-E-131–001-MY4 and NSTC 111–2221-E-131–019-MY3).

Appendix A. Supporting information

Supplementary data associated with this article can be found in the online version at doi:10.1016/j.colsurfa.2025.138120.

Data availability

No data was used for the research described in the article.

References

[1] M.P. Lutolf, Spotlight on hydrogels, Nat. Mater. 8 (6) (2007) 451–453.
[2] E.M. Ahmed, Hydrogel: preparation, characterization, and applications: a review, J. Adv. Res. 6 (2) (2015) 105–121.

[3] C. Yang, Z. Suo, Hydrogel ionotronics, Nat. Rev. Mater. 3 (6) (2018) 125–142.
[4] Y.S. Zhang, A. Khademhosseini, Advances in engineering hydrogels, Science 356 (6337) (2017) eaaf3627.
[5] O. Wichterle, D. Lim, Hydrophilic gels for biological use, Nature 185 (4706) (1960) 117–118.
[6] K.Y. Lee, D.J. Mooney, Hydrogels for tissue engineering, Chem. Rev. 101 (7) (2001) 1869–1880.
[7] J.L. Drury, D.J. Mooney, Hydrogels for tissue engineering: scaffold design variables and applications, Biomater 24 (24) (2023) 4337–4351.
[8] R.P. Lanza, R.S. Langer, J. Vacanti, A. Atala, Principles of tissue engineering, Academic Press, 2020. ISBN 978-0-12-818422-6.
[9] R. Langer, J.P. Vacanti, C.A. Vacanti, A. Atala, L.E. Freed, G. Vunjak-Novakovic, Tissue engineering: biomedical applications, Tissue Eng. 1 (2) (1995) 151–161.
[10] T. Dvir, B.P. Timko, D.S. Kohane, R. Langer, Nanotechnological strategies for engineering complex tissues, Nat. Nanotechnol. 6 (1) (2011) 13–22.
[11] S. Talebian, M. Mehrali, N. Taebnia, C.P. Pennisi, F.B. Kadumudi, J. Foroughi, M. Hasany, M. Nikkhah, M. Akbari, G. Orive, A. Dolatshahi-Pirouz, Self-healing hydrogels: the next paradigm shift in tissue engineering? Adv. Sci. 6 (2019) 1801664.
[12] K.J. Rambhia, P.X. Ma, Controlled drug release for tissue engineering, J. Contr. Release 219 (3) (2015) 119–128.
[13] A.D. Theocharis, S.S. Skandalis, C. Gialeli, N.K. Karamanos, Extracellular matrix structure, Adv. Drug Deliv. Rev. 97 (2016) 4–27.
[14] C. Frantz, K.M. Stewart, V.M. Weaver, The extracellular matrix at a glance, J. Cell Sci. 123 (24) (2010) 4195–4200.
[15] F.T. Bosman, I. Stamenkovic, Functional structure and composition of the extracellular matrix, J. Pathol. 200 (4) (2003) 423–428.
[16] A.O. Eghrari, S.A. Riazuddin, J.D. Gottsch, Overview of the cornea: structure, function, and development, Prog. Mol. Biol. Transl. Sci. 134 (2015) 7–23.
[17] E.M. Espana, D.E. Birk, Composition, structure and function of the corneal stroma, Exp. Eye Res. 198 (2020) 108137.
[18] G.A. Holzapfel, Determination of material models for arterial walls from uniaxial extension tests and histological structure, J. Theor. Biol. 238 (2) (2006) 290–302.
[19] R.M. Nerem, Vascular fluid mechanics, the arterial wall, and atherosclerosis, J. Biomech. Eng. 114 (3) (1992) 274–282.
[20] I. Hariton, G. Debotton, T.C. Gasser, G.A. Holzapfel, Stress-driven collagen fiber remodeling in arterial walls, Biomech. Model. Mechanobiol. 6 (2007) 163–175.
[21] J.M. Mattson, R. Turcotte, Y. Zhang, Glycosaminoglycans contribute to extracellular matrix fiber recruitment and arterial wall mechanics, Biomech. Model. Mechanobiol. 16 (2017) 213–225.
[22] G.A. Holzapfel, T.C. Gasser, R.W. Ogden, A new constitutive framework for arterial wall mechanics and a comparative study of material models, J. Elast. 61 (2000) 1–48.
[23] L.H. Timmins, Q. Wu, A.T. Yeh, J.E. Moore Jr, S.E. Greenwald, Structural inhomogeneity and fiber orientation in the inner arterial media, Am. J. Physiol. Heart Circ. Physiol. 298 (5) (2010) H1537–H1545.
[24] M.W. Tibbitt, K.S. Anseth, Hydrogels as extracellular matrix mimics for 3D cell culture, Biotechnol. Bioeng. 103 (4) (2009) 655–663.
[25] H. Geckil, F. Xu, X. Zhang, S. Moon, U. Demirci, Engineering hydrogels as extracellular matrix mimics, Nanomed 5 (3) (2010) 469–484.
[26] M. Zhang, S. Xu, R. Wang, Y. Che, C. Han, W. Feng, C. Wang, W. Zhao, Electrospun nanofiber/hydrogel composite materials and their tissue engineering applications, J. Mater. Sci. Technol. 162 (2023) 157–178.
[27] J.W. Lee, K.H. Song, Fibrous hydrogels by electrospinning: novel platforms for biomedical applications, J. Tissue Eng. 14 (2023), 20417314231191881.
[28] Y. Su, M.S. Toftdal, A. Le Friec, M. Dong, X. Han, M. Chen, 3D electrospun synthetic extracellular matrix for tissue regeneration, Small Sci. 1 (2021) 2100003.
[29] F.A. Formica, E. Öztürk, S.C. Hess, W.J. Stark, K. Maniura-Weber, M. Rottmar, M. Zenobi-Wong, A bioinspired ultraporous nanofiber-hydrogel mimic of the cartilage extracellular matrix, Adv. Healthc. Mater. 5 (24) (2016) 3129–3138.
[30] S. Deepthi, M. Nivedhitha Sundaram, J. Deepti Kadavan, R. Jayakumar, Layered chitosan-collagen hydrogel/aligned PLLA nanofiber construct for flexor tendon regeneration, Carbohydr. Polym. 153 (2016) 492–500.
[31] H. Gong, C. Bao, X. Guo, F. Tian, L. Qiu, W. Yang, A universal electrochemical sensor for detection of nucleic acids and protein based on host-guest recognition of β-cyclodextrin polymer, Microchem. J. 204 (2024) 110987.
[32] X. Luo, S. Cui, W. Yang, Y. Yu, An electrochemical quinine detection approach based on small molecule promoted split aptamer click ligation reaction, Talanta 292 (2025) 127916.
[33] L. Li, F. Tian, F. Wu, L. Qiu, S. Geng, M. Li, Z. Chen, W. Yang, Y. Liu, Y. Yu, Strong electronic metal-support interaction of Ni4Mo/N-SrMoO4 promotes alkaline hydrogen electrocatalysis, Appl. Catal. B Environ. 361 (2025) 124660.
[34] X. Ren, L. Qiu, M. Li, F. Tian, L. He, X. Guo, F. Wu, Y. Liu, J. Sheng, W. Yang, Y. Yu, Hierarchically interfacial sulfide/phosphides achieve industry-level water electrolyzer in alkaline conditions at 3A cm-2. appl. Catal. B: environ 378 (2025) 125622.
[35] B. Sarker, R. Singh, R. Silva, J.A. Roether, J. Kaschta, R. Detsch, D.W. Schubert, I. Cicha, A.R. Boccaccini, Evaluation of fibroblasts adhesion and proliferation on alginate-gelatin crosslinked hydrogel, Plos One 9 (9) (2014) e107952.
[36] B.; Sarker, J.; Rompf, R.; Silva, N.; Lang, R.; Detsch, J.; Kaschta, B. Fabry, A. R. Boccaccini, Alginate-based hydrogels with improved adhesive properties for cellencapsulation, Int. J. Biol. Macromol. 78 (2015) 72–78.
[37] B. Kanti Das, R. Samanta, S. Ahmed, B. Pramanik, Disulphide cross-linked ultrashort peptide hydrogelator for water remediation, Chem. Eur. J. 29 (2023) e202300312.
[38] C. Duan, H. Jiang, S. Zhang, Y. Wang, P. Liu, B. Xu, W. Tian, B. Han, Construction of strontium-loaded injectable lubricating hydrogel and its role in promoting repair of cartilage defects, Biomater. Sci. 13 (2025) 1449–1463.
[39] M. Rosa, E. Gallo, P. Pellegrino, F.A. Mercurio, M. Leone, M. Cascione, B. Carrese, G. Morelli, A. Accardo, C. Diaferia, Inclusion of cationic amphiphilic peptides in fmoc-FF generates multicomponent functinal hydrogels, ACS Appl. Bio Mater. 8 (2025) 488–502.
[40] Y.H. Tseng, T.L. Ma, D.H. Tan, A.-J.A. Su, K.M. Washington, C.C. Wang, Y. C. Huang, M.C. Wu, W.F. Su, Injectable hydrogel guides neurons growth with specific directionality, Int. J. Mol. Sci. 24 (2023) 7952.
[41] T.L. Ma, S.C. Yang, T. Cheng, M.Y. Chen, J.H. Wu, S.L. Liao, W.L. Chen, W.F. Su, Exploration of biomimetic poly(γ-benzyl-l-glutamate) fibrous scaffolds for corneal nerve regeneration, J. Mater. Chem. B 10 (2022) 6372–6379.
[42] K.H. Wang, C.H. Liu, D.H. Tan, M.P. Nieh, W.F. Su, Block sequence effects on the self-assembly behaviors of polypeptide-based penta-block copolymer hydrogels, ACS Appl. Mater. Interfaces 16 (5) (2024) 6674–6686.
[43] Y.; Liu, L.; Wang, L. Zhao, Y.; Zhang, Z.T.; Li, F. Huang, Multiple hydrogen bonding driven supramolecular architectures and their biomedical applications, Chem. Soc. Rev. 53 (2024) 1592–1623.
[44] T.L. Ma, C.M. Tsai, S.C.; Luo, W.L. Chen, Y.C. Huang, W.F. Su, Chemical structures and compositions of peptide copolymer films affect their functional properties for cell adhesion and cell viability, React. Funct. Polym. 175 (2022) 105265.
[45] T.L. Ma, S.C. Yang, S.C. Luo, W.L. Chen, S.L. Liao, W.F. Su, Dual-function fibrous co-polypeptide scaffolds for neural tissue engineering, Macromol. Biosci. 23 (2022) 2200286.
[46] J. Chen, R.N. Dong, J. Ge, B.L. Guo, P.X. Ma, Biocompatible, biodegradable, and electroactive polyurethane-urea elastomers with tunable hydrophilicity for skeletal muscle tissue engineering, ACS Appl. Mater. Interfaces 7 (51) (2015) 28273–28285.
[47] T.G. Tihan, M.D. Ionita, R.G. Popescu, D. Iordachescu, Effect of hydrophilic-hydrophobic balance on biocompatibility of poly(methyl methacrylate) (PMMA)-hydroxyapatite (HA) composites, Mater. Chem. Phys. 118 (2-3) (2009) 265–269.
[48] C.C. Wu, C.K. Wei, C.C. Ho, S.J. Ding, Enhanced hydrophilicity and biocompatibility of dental zirconia ceramics by oxygen plasma treatment, Mater 8 (2) (2015) 684–699.